Hindawi
Wireless Communications and Mobile Computing
Volume 2022, Article ID 7939777, 9 pages
https://doi.org/10.1155/2022/7939777

Research Article

Application of a Wind Environment Simulation Generation Technology in Urban Planning

Yang Chen

College of Art and Design, Hunan First Normal University, Changsha, Hunan 410000, China

Correspondence should be addressed to Yang Chen; shy@hnfnu.edu.cn

Received 14 June 2022; Revised 18 July 2022; Accepted 21 July 2022; Published 12 August 2022

Academic Editor: Kalidoss Rajakani

With the acceleration of urbanization, cities have shown a development trend of high density, high height, and high intensity, which significantly weakens the airflow in the city, resulting in the accumulation of heat and pollutants, and in the urban environment, the problem is getting worse. Therefore, it is particularly necessary to strengthen urban ventilation in the urban environment. However, in the real urban environment, the building layouts are diverse, the building forms are different, and the interaction of the building wind environment is complex due to the lack of relevant research on the complex building spatial form in the urban mesoscale area on the outdoor pedestrian. The research results are difficult to be applied in actual urban construction, and it is difficult to guide the optimization of the urban wind environment. To solve this problem, this paper adopts the CFD method in a real-scale (1 : 1) urban mesoscale regional wind environment simulation study. On this basis, the influencing factors of the urban pedestrian wind environment are analyzed, and the optimization strategy of the wind environment is proposed, which can provide practical guidance for the planning practice of enhancing urban wind comfort.

1. Introduction

As the level of economic and social development continues to rise, the process of industrialization and urbanization around the world continues to accelerate. According to the World Urbanization Prospects, the proportion of the global urban population has exceeded 48% and is growing at an average annual rate of 1.9% [1]. At the same time, China's urbanization level has been increasing year by year in the past decade. As of 2019, China's urban population has increased from 645.12 million in 2009 to 848.43 million, and its proportion in the total population has increased from 48.34% to 60.60% [2]. Vigorous urban development has improved the living standards of residents to a certain extent, but it has also increased the burden on the environment, bringing about environmental problems such as poor urban ventilation, the heat island effect, and the accumulation of pollutants [3].

On the one hand, the development of urban complex architectural spatial forms increases the urban roughness, which in turn exacerbates the complexity of turbulent motion near the ground. Studies have shown that under the influence of buildings, the air forms around the buildings, such as downdrafts, wakes, and angular flows, which will affect people's outdoor work and activities [4]. On the other hand, due to the extensive use of artificial construction materials and the reduction of urban blue-green space (water bodies and green space in the city), the structure of the urban underlying surface has changed, resulting in the reduction of turbulent heat transfer in the urban boundary layer, and the urban heat dissipation and moisture storage capacity decreases; at the same time, the heat generated by humans is frequently emitted, which increases the heat inside the city and makes the urban heat island effect more pronounced [5].

Studies have shown that the urban heat island effect will not only affect the thermal comfort of urban residents but also lead to an increase in air-conditioning energy consumption and even lead to an increase in population mortality [6].

In this context, strengthen urban ventilation to make the city "breathe" better. Creating a good urban wind environment can not only alleviate the urban heat island effect and

meet the outdoor human comfort requirements of residents but also reduce the generation of unfavorable wind conditions around the building, promote the diffusion of pollutants, and improve the air quality in residential areas and buildings [7]. However, in the current urban planning and construction, too much attention is paid to the single building form, but the relationship between the complex architectural spatial form and the wind field in the large-scale building group is ignored. Design and architectural layouts are addressed [8].

However, my country lacks corresponding regulations and standards to specify the outdoor wind environment, and urban planners also lack scientific means to study and evaluate the wind environment of complex architectural spatial forms in urban mesoscale areas [9]. Therefore, in a modern city with high-density development, using scientific means to accurately predict and optimize the urban wind environment has important practical significance for the sustainable development of the city and urban planning and design [10].

2. State of the Art

2.1. The Concept of the Wind Environment

2.1.1. Forming Factors. The wind environment refers to the wind field formed by the outdoor natural wind under the influence of the urban landform or natural landform. At present, the wind environment is mainly studied in the scientific field of architectural design and urban planning. The wind environment acts on the outdoor natural wind conditions and is a wind field formed by the influence of the urban topography [11]. The formation of the wind environment is complex and changeable, and it is formed under the influence of many aspects of the earth's surface [12]. Firstly, the flow of gas caused by the influence of the atmosphere is one of the reasons for the formation of wind [13]. Secondly, the atmospheric circulation in the equator, the north and south poles, and the local winds including monsoons, sea-land winds, and canyon winds are responsible for the entire wind environment (main classification). Finally, under the action of urban construction planning, mechanized turbulent motion caused by buildings of different heights, trees, and terrain differences is also one of the factors that form the wind environment [14].

2.1.2. Definition of Wind Parameters. According to the content of "Chinese Standard Weather Data for Building Thermal Environment Analysis" (Chinese Standard Weather Data (CSWD)), the country takes the wind speed and wind direction as the research object, establishes the intensity level and direction of wind, and selects 16 numbers. It expresses the wind direction and azimuth, in which 0 means still wind, and the specific corresponding relationship is shown in Table 1.

2.2. Research Methods of the Urban Wind Environment. The research methods of the urban wind environment are roughly three types. The convenience and practicability of each research method are different in different research scales and research contents [15]. Among them, the measured data is analyzed at the macroscale (the research scale is usually in urban areas of 10 km to 100 km), the mesoscale (the research scale is usually in the range of 10 km~100 km) [16], and the microscale (the research scale is usually in the single building, building array, and street valley area in the range of 10 m to 1 km), and it mainly studies the distribution of a single building [17]. Analyze the wind comfort in the valley and urban areas. The wind tunnel test mainly conducts the qualitative and quantitative analysis of the micro- and mesoscale of urban areas. Computational fluid dynamics (CFD) numerical simulation mainly studies the wind fields of single buildings, street valleys, and building complexes at the microscale time; meanwhile, the WRF (Weather Research and Forecasting) model is used. Wind field studies in urban mesoscale regions are also carried out in conjunction with CFD simulations [18].

2.2.1. Field Measurements. Field measurement plays a vital role in urban wind environment research because it can obtain the basic data of the research object in the actual environment. Field measurements can directly reflect the air movement in the city and are widely used in research and analysis of various scales. In the macroscale meteorological movement, detailed wind and heat field data are obtained mainly by collecting and analyzing scattered weather stations and satellite data [19].

However, due to the high cost of equipment, it has not been widely used. Similar to the studies at the macroscale, the studies of the urban wind environment at the mesoscale mainly collect data from small weather stations and satellites. In the microscale research of individual buildings, street valleys, and small-scale building groups, field measurement technologies such as infrared imaging and scattered wind and heat data acquisition are widely used [20].

In addition, measurement technologies such as scattered point data collection, infrared imaging, and high-speed cameras are also efficient means of measuring the indoor wind environment of buildings. Kitous et al. took the macroscale city of Gerhardia as the research object and used the field scatter measurement method to discuss the impact of complex terrain and urban layouts on the urban wind and heat environment. Zhang Bohua et al. took mesoscale residential quarters and explored the spatial layout of the quality of the wind environment through field measurement of the wind environment. By collecting data from weather stations, Cui et al. studied the wind and heat environment around different U-shaped street valleys in the ancient city of Xi'an and conducted an on-site assessment of the pedestrian-level air quality. Zhang Kang took the factory in the Suzhou area as a typical case and used an on-the-spot measurement method to explore the indoor wind environment of the factory in different regions.

Although field measurement methods are widely used in urban wind environments and can accurately collect primary data, they still have some drawbacks. For example, in a specific test environment, whether the data analysis conclusions obtained through limited collection points are representative still needs to be demonstrated; at the same

Table 1: Correspondence table of the wind direction and azimuth.

Wind direction	N	NNE	NE	ENE	E	ESE	SE	SSE	S	SSE	SW	WSW	W	WN	NW	NNW	Calm wind
Position	1	2	3	4	5	6	7	8	9	10	11	12	13	14	15	16	0

time, whether the conclusions under specific test conditions are general still needs to be discussed.

In addition, due to the difficulty in controlling the test environment in field measurement, factors such as test parameters, the number of measurement points, the accuracy of measurement instruments, measurement methods, and time affect the quality and value of the field measurement results. Therefore, high-quality and high-value field measurement research requires an enormous investment in equipment, manpower, and time.

2.2.2. Wind Tunnel Test. The wind tunnel experiment in fluid mechanics refers to an aerodynamic experiment method in which an aircraft or other object model is placed in the wind tunnel to study the gas flow and its interaction with the model so as to understand the aerodynamic characteristics of the actual aircraft or other objects. The wind tunnel test is a method to study large-scale phenomena through microscale experiments in an artificially simulated atmospheric environment by using a scale model based on similar principles. Wind tunnel tests were widely used in the field of research in the 1890s, mainly in the microscale wind environment analysis and research of single buildings, building groups, and blocks with a horizontal diameter of less than 1 km.

Usually, measurement methods include hot wire or hot film technology, pulsed hot wire technology, and probe technology. The wind field characteristics with the relatively precise location make the wind tunnel tests have significant advantages in the study of the urban wind environment.

Tse et al. took a single building as the research object and used a laser Doppler anemometer to explore the change of the single building at different deflection angles of the wind direction. Weerasuriya et al. conducted a wind tunnel experimental study using a laser Doppler anemometer to explore the ventilation efficiency and wind speed levels at pedestrian heights around one and more groups of buildings. Allegrini et al. used a particle image velocimeter to conduct a 1 : 400 wind tunnel test study to explore the wind speed distribution and turbulence in the building passage under different angles of the building form.

It is not difficult to find that the above measurement techniques can only perform "point measurement." Although LDA and PIV technologies can perform 3D real-time monitoring, they are expensive, and the laser is easily blocked by scale models, making it difficult to achieve 3D measurement of the entire flow field in urban areas. At the same time, wind tunnel tests need to follow similar criteria, and the costs of personnel, equipment, and models for wind tunnel tests are relatively high, which limits the large-scale application of wind tunnel tests to a certain extent.

2.2.3. Computer Numerical Simulation. The comprehensive analysis has been widely used in many fields such as single buildings, wind environment and parameter research around buildings, urban street valley wind environment assessment, and pollutant diffusion research. Gong Bo used CFD numerical simulation to explore the wind and heat building under different wind directions and building spacing. Taking a large commercial building as the research object, Du Xiaolei et al. used CFD numerical simulation to analyze and evaluate the wind and heat environment around the building. Cai Yadong et al. used the Reynolds average method to study the overall and local pedestrian wind comfort in a university in Changchun. Huang Wenfeng et al. took the typical building group as the research object and used the Reynolds average method to study the wind environment around the building group under different wind directions and different building layouts. Fan et al. used a standard k-ε model based on the Reynolds average equation to study the air quality and pedestrian wind comfort in isolated and nonisolated street canyons with different opening structures.

In addition, the WRF model (a mesoscale weather forecast model) is also used in urban wind environment research, and its simulation results are usually used for CFD numerical simulation, and then the research in urban areas is carried out. By coupling WRF and CFD numerical simulation methods, Shen Lian et al. revealed the distribution law of wind fields in urban communities with different incoming winds. Temel et al. provided inflow conditions for the complex terrain of Riad City in Spain through a mesoscale WRF model and used the CFD method to explore the wind flow in the Riad Ferrol Channel. Hu Shasha and others used WRF and CFD methods to analyze the heat environment in the urban area of Huangshi and determined the layout of the air ducts in this area. Compared with the field measurement and wind tunnel test, the numerical simulation represented by CFD can realize the comparative analysis of a large number of different case results. It has the advantages of low computational costs and higher visualization of results. However, the accuracy of CFD simulation results is affected by many parameters such as governing equations, turbulence models, computational domain sizes, boundary conditions, and convergence criteria.

Therefore, in related research, the field measurement, wind tunnel test, and CFD simulation are usually combined: the field measurement provides basic boundary conditions and other parameter data for CFD simulation, the wind tunnel test provides verification data for CFD simulation, and the CFD simulation provides the wind environment. The study provides multiparameter and full flow field analysis

data. Jiang Sicheng et al. took a street valley in an old urban area as the research object, provided boundary conditions and other parameters for CFD simulation through the climatic characteristics of field observations, and studied the aspect ratio and direction of different streets on the internal wind environment of the street valley. Ma Mengyao studied the outdoor pedestrian wind environment of a gymnasium by combining the on-the-spot measurement and CFD numerical simulation method. Yang Liguo et al. took a ski resort, used the CFD numerical simulation method to explore the influence of the complex terrain in this area, and used the wind tunnel test results to verify and explain.

3. Establishment and Verification of the CFD Numerical Model

3.1. Area Selection. Before simulating the wind environment of the outdoor building group, the actual measurement method should be used to compare the wind speed to verify the accuracy of the Airpak software simulation.

Shanghai has four distinct seasons, a mild climate, abundant sunshine and rainfall, and a subtropical monsoon climate. Influenced by the geographical location, Shanghai has the longest characteristics in summer, followed by winter, and the shortest in spring and autumn. In summer, under the action of the Pacific subtropical high, the Shanghai area is mostly southeasterly, and the weather is hot and humid. In winter, it is controlled by the cold high pressure of Siberia, prevailing northwesterly winds, and the weather is cold and dry. The main meteorological disasters in Shanghai include strong winds, typhoons, fog, haze, thunderstorms and floods, high temperature and heat waves, and cold waves. The four-month flood season begins in June, and its characteristics can be summarized as the increase in the total amount of precipitation, the increase in the amount of plum rain, the increase in the number of high-temperature days, and the increase in the number of typhoons as shown in Figure 1.

With the wind speed over the past 2000-2020 released by the Shanghai Meteorological Bureau in Figure 2, the overall trend of the average wind speed and maximum wind speed statistics in Shanghai in the past 20 years is stable, the average wind speed is 3.06 m/s, and the maximum is 5.59 m/s. From 2000 to 2005, the city's average wind speed showed an upward trend. The highest average wind speed in five years appeared in 2004 and 2005, and the wind speed was both 3.62 m/s. Since 2006, the average wind speed in Shanghai has been decreasing, but the decrease is not large, and the average wind speed remains at 3 m/s. Overall, the lowest wind speed in the first 10 years in Shanghai appeared in 2002, speed of 3.05 m/s, and the lowest value per minute in the last 10 years appeared in 2020, speed of 2.56 m/s. The overall trend of the maximum wind speed in Shanghai in the past 20 years is similar to the overall trend of the average wind speed. Since 2003, the value range has increased significantly. In 2004, the high value of the maximum wind speed was 6.38 m/s, and then it began to decline significantly in 2005. The low value of the maximum wind speed appeared in 2002 with a wind speed value of 5.4 m/s. In 2010, a new

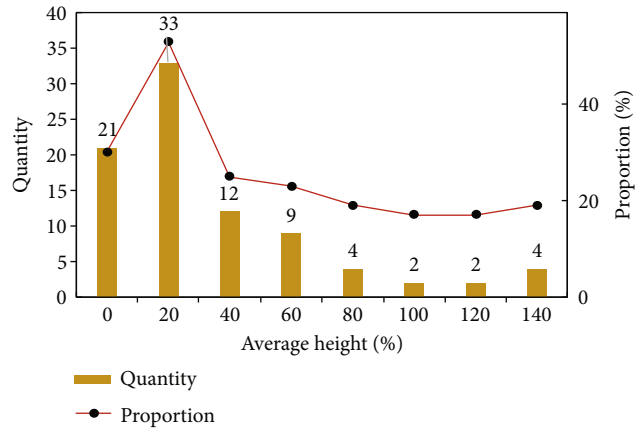

Figure 1: Statistical distribution of the average height of plots in the study area.

round of high wind speed was ushered in, with a maximum wind speed of 5.72 m/s. In the next 10 years, the increase in wind speed was not obvious, and the lowest value of the maximum wind speed appeared in 2020, with a wind speed value of 4.87 m/s.

3.2. Establishment of the CFD Numerical Model. Building clusters affect the flow of wind. When the wind flows to the building complex, physical phenomena such as friction, collision, separation, and adhesion circulation are generated with the surrounding building complex, and a tiny airflow field is formed around the building complex. The airflow generated by the building is a low-speed incompressible turbulent flow, which conforms to the Boussinesq hypothesis. In the simulation, the standard RNG model is used to solve the wind environment around the building. The control equations and momentum conservation equation are as follows:

(1) Continuity equation

For incompressible fluids whose fluid density is constant, the equation simplifies to

$$\frac{\partial u_i}{\partial x_i} = 0. \tag{1}$$

In the formula, u_i is the speed i.

(2) Momentum conservation equation

$$\frac{\partial}{\partial x_j}\left(\rho u_i u_j\right) = \frac{\partial p}{\partial x_i} + \frac{\partial \tau_{ij}}{\partial x_j} + \rho g_i + F_i. \tag{2}$$

In the formula, ρ is the density, p is the pressure, τ_{ij} is the tensor, ρg_i is the force, and F_i is the heat source, and we also have the pollution source term due to the

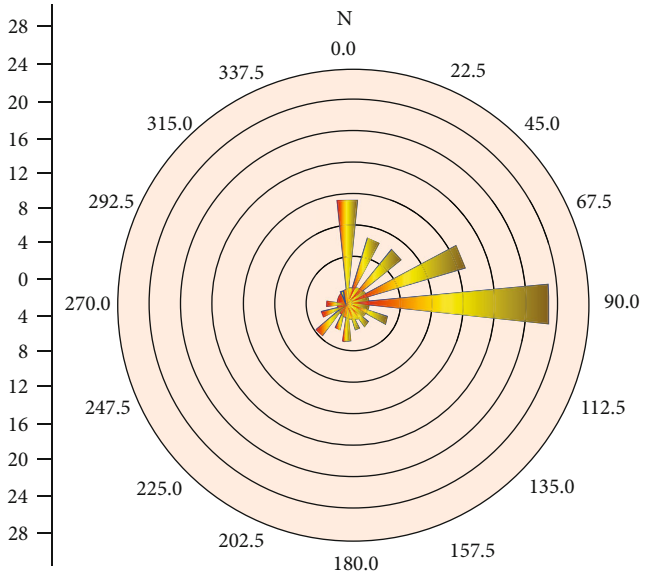

Figure 2: Statistics of the average wind speed and maximum wind speed in Shanghai (2000-2020).

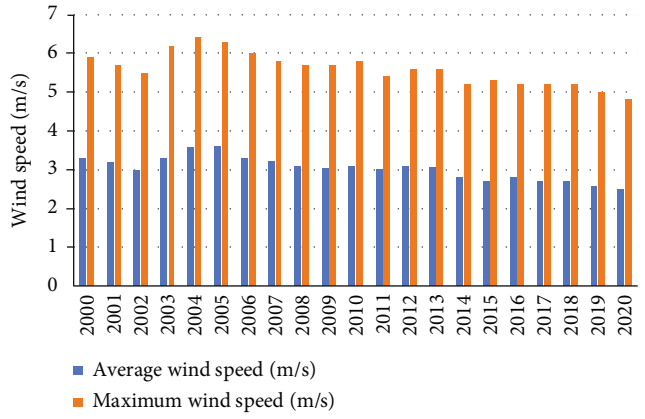

Figure 3: Directional probability distribution of the annual wind speed in Shanghai (1953-2000).

contamination source, etc., of which,

$$\tau_{ij} = \mu\left[\frac{\partial u_i}{\partial x_j} + \frac{\partial u_j}{\partial x_i}\right] - \frac{2}{3}\mu\frac{\partial u_i}{\partial x_i}\delta_{ij}, \tag{3}$$

where μ is the viscosity, and the above formula (3) is the volume diffusion.

(3) Mass conservation equation

$$\frac{\partial u}{\partial x} + \frac{\partial v}{\partial y} + \frac{\partial w}{\partial z} = 0. \tag{4}$$

(4) Energy conservation equation

$$\frac{\partial u}{\partial x_i}(\rho u_i h) = \frac{\partial}{\partial x_i}(k + k_i)\frac{\partial T}{\partial x_i} + S_h, \tag{5}$$

where k is the conductivity; k_t is the thermal diffusion:

$$k_t = \frac{c_p \mu_t}{Pr_t}. \tag{6}$$

For the boundary conditions of the entrance and exit, the wind speed of the entrance flow is uniformly distributed. Different heights produce different wind speeds, and the wind speed increases with height. The formula for calculating the altitude and wind speed is as follows:

$$v_h = v_0\left(\frac{h}{h_0}\right)^n, \tag{7}$$

where v_h is the wind speed at height h, in m/s; v_0 is the wind speed at the reference height h_0, in m/s, generally taken as the wind speed at 10 m; and n is the exponent, taken as 0.33.

The strong wind area ratio R_Q is defined as

$$R_Q = \left(\frac{S_Q}{S_0}\right) \times 100\%, \tag{8}$$

where S_Q is the area occupied by the strong wind area in the flow field (m^2) and S_0 is the area (m^2) at the height of the strong wind area without interference from buildings.

In the same way, the quiet wind area is the area with a small value of urban spatial wind speed. In the urban space, it is a quiet wind area. Through the size of the area ratio index of the quiet wind area, the proportion of the poor wind environment can be judged. The quiet wind area ratio R_J is defined as

$$R_J = \left(\frac{S_J}{S_0}\right) \times 100\%. \tag{9}$$

In the formula, S_J is the area occupied by the calm wind area in the flow field (m^2) and S_0 is the area (m^2) at the height of the calm wind area when it is not disturbed by buildings.

Based on the postprocessing of the simulation results of Airpak software, Photoshop software was used to process the air age cloud map; that is, the air age values and areas represented by different color blocks were calculated, and the weighted average method was used to calculate the average air age of the study area. The mean air age A is defined as

$$\bar{A} = \frac{A_1 \times S_1 + A_2 \times S_2 + \cdots A_n \times S_n}{S_1 + S_2 + \cdots S_n}. \tag{10}$$

In the formula, A is the average air age (s), A_n is the air age represented by different color blocks, and S_n is the time spent in A_n.

Combined with the practical application of this paper, the middle wind speed ratio is used as the relative comfort zone wind speed ratio R_S to judge the size of the area at

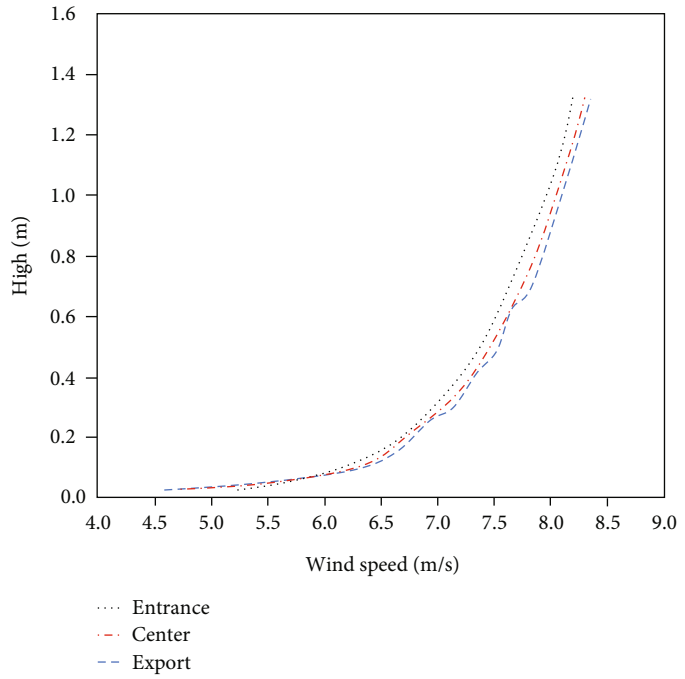

Figure 4: Wind speed at the inlet, center, and outlet profiles of the CFD computational domain.

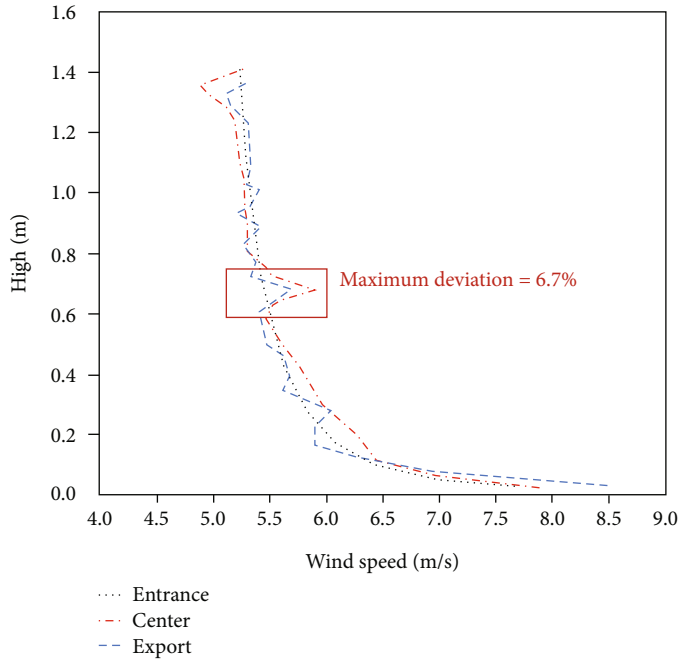

Figure 5: Turbulence intensity at the inlet, center, and outlet profiles of the CFD computational domain.

the height of 1.5 m that meets the comfort of outdoor pedestrians. The relative comfort zone wind speed ratio R_S is defined as

$$R_S = 1 - R_Q - R_J. \tag{11}$$

The inlet wind profile is set through user-defined functions. The inlet vertical velocity boundary condition is modified based on the exponential law wind speed profile model combined with the wind tunnel test, regardless of the wind direction difference, and the final wind speed profile is

$$V = 7.5 \times \left(\frac{Z}{0.6}\right)^{0.11}. \tag{12}$$

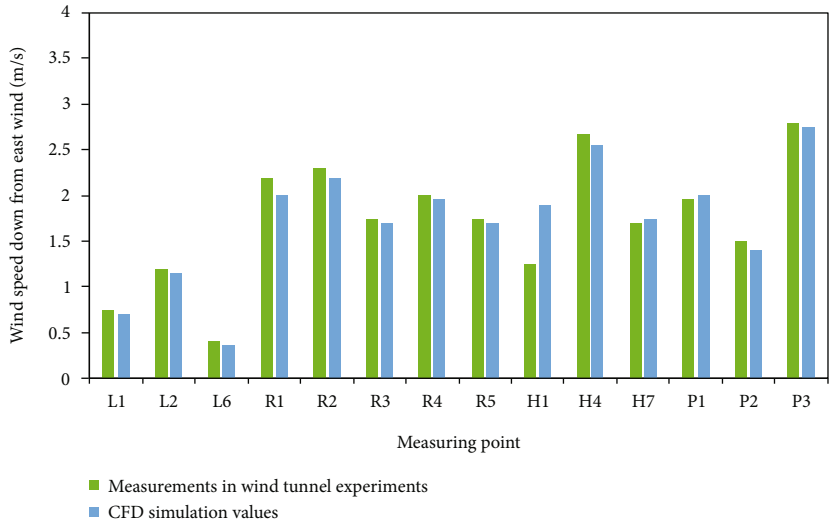

Figure 6: Comparison of CFD simulation results with wind tunnel test measurements: east wind.

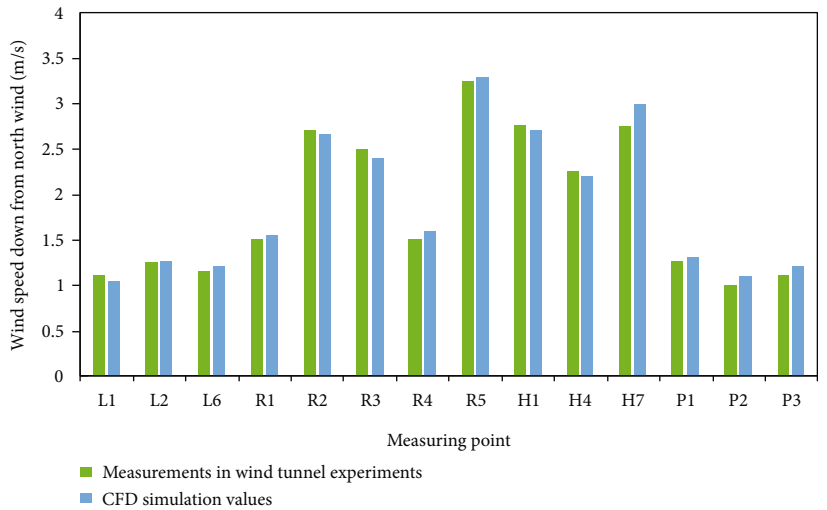

Figure 7: Comparison of CFD simulation results with wind tunnel test measurements: north wind.

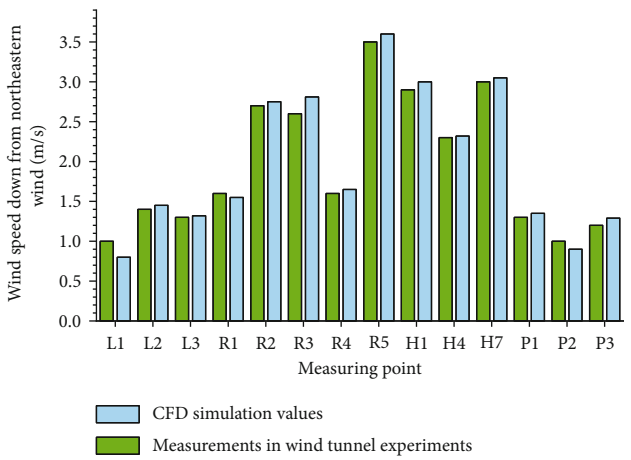

Figure 8: Comparison of CFD simulation results with wind tunnel test measurements: northeastern wind.

The governing equation of the LES model is

$$\frac{\partial}{\partial t}\left(\rho\overline{u_i}\right) + \frac{\partial}{\partial X_j}\left(\rho\overline{u_i u_j}\right) = \frac{\partial}{\partial X_j}\left(\mu\frac{\partial\overline{u_i}}{\partial X_j}\right) + \frac{\partial\bar{p}}{\partial X_i} - \frac{\partial\tau_{ij}}{\partial X_j}, \quad (13)$$

where τ_{ij} is the subgrid stress, defined as

$$\tau_{ij} = \rho\overline{u_i u_j} - \rho\overline{u_i}\cdot\overline{u_j}. \quad (14)$$

The eddy viscosity calculation equation in the Smagorinsky-Lilly model is

$$\mu_t = \rho L_S^2\left|\bar{S}\right|. \quad (15)$$

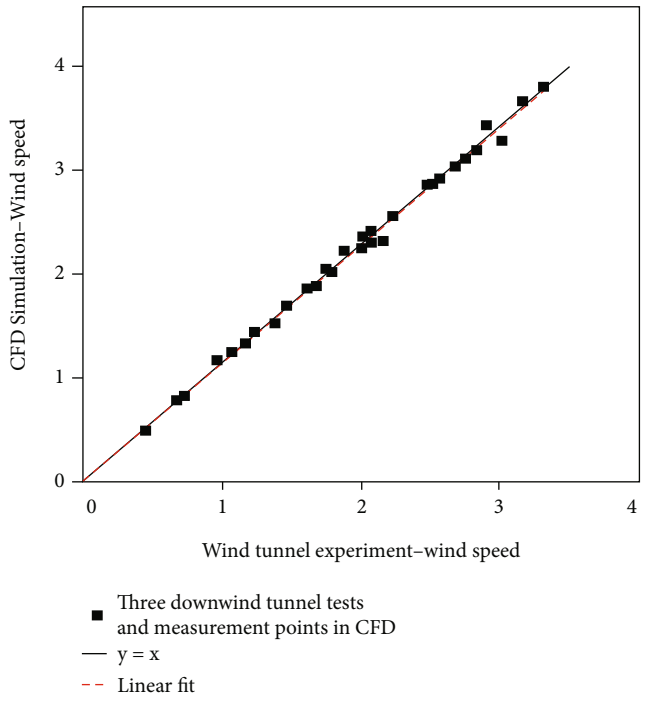

Figure 9: Comparison of CFD simulation results with wind tunnel test measurements: linear fit.

4. Experimental Results and Analysis

When studying the urban outdoor wind environment, this study adopts the LES model for the incompressible unsteady flow. The velocity inflow boundary and pressure outlet are selected. The inflow boundary is the gradient wind distributed along the height index, which is realized by the UDF setting. The inflow wind direction is realized by rotating the corresponding angle of the study area; the two sides and the top of the computational domain have zero shear stress, which can significantly improve the calculation. It has stability and little impact on the calculation results; the ground and building walls are set as nonslip walls; for the SIMPLE algorithm, the standard format type is used for the others, and the calculation time step is 0.004 s. The residual error of convergence to the continuity equation is less than 10*e*-03, and the residual error of each velocity component is less than 10*e*-04.

According to the research of Weerasuriya et al., the directional probability distribution of nontyphoon wind speed in Shanghai (1953-2000) was obtained (Figure 3). In this paper, three prevailing wind directions of easterly 90°, northerly 0°, and northeasterly 292.5° were selected for numerical simulation research.

4.1. Horizontal Homogeneity Test of the Flow Field. The atmospheric boundary layer should maintain horizontal homogeneity between upstream and downstream, so the inflow characteristics of computational fluid dynamics (CFD) simulations should be stable throughout the computational domain. In this study, the CFD numerical simulation of the wind tunnel test flow was carried out in a blank computational domain, and the flow characteristics (wind speed, turbulence intensity) at the center were extracted and compared with the inflow characteristics. As shown in Figures 4 and 5, the CFD model established in this study basically meets the requirements of horizontal homogeneity. The wind speed characteristic curves of the inlet, center, and outlet are basically consistent (Figure 4); although the turbulence intensity curve deviates slightly (Figure 5), the maximum deviation is 6.7% (the box position in Figure 5), which is less than 7%, which is within the acceptable range.

4.2. Model Validation Results. In this study, the measured values of Weerasuriya et al. and other wind tunnel tests are compared with the CFD results of three wind directions. The positions of 14 measurement points in the wind tunnel test are shown in Figures 6 and 7. The CFD results of 14 measurement points in three wind directions are very close to the results in the test (Figure 8).

By linearly fitting the CFD simulation and the measured values of the test, it is found that most of the points are located on the $y = x$ line, indicating the CFD values of the wind tunnel test as shown in Figure 9.

5. Conclusion

(1) Through the UDF setting, the inflow wind direction is achieved by rotating the corresponding angle of the study area. The two sides and the top of the calculation domain have zero shear stress, which can significantly improve the calculation. It has good stability and little influence on the calculation results. The ground and building walls are set as antiskid walls. Other algorithms adopt the SIMPLE algorithm of standard format, and the calculation time step is 0.004 s. The residual error converging to the continuity equation is less than 10*e*-03, and the residual error of each velocity component is less than 10*e*-04

(2) In this paper, three prevailing wind directions, east wind 90°, north wind 0°, and northeast wind 292.5°, are selected for numerical simulation research. The CFD model established in this study basically meets the requirements of horizontal uniformity. The wind speed characteristic curves at the inlet, center, and outlet are basically the same (Figure 4). Although the turbulence intensity curve has a slight deviation (Figure 5), the maximum deviation is 6.7% (the box position in Figure 5), which is less than 7%, which is within the acceptable error range. Through the linear fitting of the CFD simulation and experimental measurements, it is found that most points are located on the $y = x$line. The complex characteristics of airflow around buildings significantly affect the local wind field changes and the distribution of the wind velocity ratio. At the same time, due to the weakening of the blocking effect of low-rise buildings on the wind, the wind speed ratio of the field will increase significantly

Data Availability

The figure and table data used to support the findings of this study are included in the article.

Conflicts of Interest

The author declares that there are no conflicts of interest.

References

[1] G. Cremen, C. Galasso, and J. Mccloskey, "A simulation-based framework for earthquake risk-informed and people-centered decision making on future urban planning," *Earth's Future*, vol. 10, no. 1, pp. 178–185, 2022.

[2] C. Ogilvie, J. Ospina, C. Konstantinou et al., "Modeling communication networks in a real-time simulation environment for evaluating controls of shipboard power systems," in *2020 IEEE CyberPELS (CyberPELS)*, vol. 45no. 4, pp. 732–738, Miami, FL, USA, 2020.

[3] T. Jaakkola and K. Veermans, "Learning electric circuit principles in a simulation environment with a single representation versus "concreteness fading" through multiple representations," *Computers & Education*, vol. 148, no. 23, article 103811, 2020.

[4] S. Iqbal, T. Ardalan, M. Hadi, and E. Kaisar, "Developing guidelines for implementing transit signal priority and freight signal priority using simulation modeling and a decision tree algorithm," *Transportation Research Record*, vol. 2676, no. 4, pp. 133–144, 2022.

[5] M. T. Le and I. S. Shukurov, "Computational fluid dynamics analysis for thermal-wind environment simulation of urban street in Hanoi city," vol. 16, no. 7, pp. 77–85, 2020.

[6] O. A. Rastyapina, V. G. Polyakov, V. V. Prokopenko, O. A. Ganzha, and T. A. Sabitova, "Analysis and assessment of urban planning safety to achieve sustainable development of urban planning environment," *E3S Web of Conferences*, vol. 208, p. 04012, 2020.

[7] B. Halder and J. Bandyopadhyay, "Evaluating the impact of climate change on urban environment using geospatial technologies in the planning area of Bilaspur, India - ScienceDirect," *Environmental Challenges*, vol. 34, no. 11, article 100702, 2021.

[8] O. Chinedu, O. Gozie, and O. Arinze, "CFD analysis of wind-induced pollutant dispersion in built environment," vol. 14, no. 2, pp. 991–1009, 2021.

[9] A. Coppola, L. D. Costanzo, L. Pariota, S. Santini, and G. N. Bifulco, "An integrated simulation environment to test the effectiveness of GLOSA services under different working conditions," *Transportation Research Part C: Emerging Technologies*, vol. 134, p. 103455, 2022.

[10] A. K. Bairagi and S. K. Dalui, "Wind environment around the setback building models," *Building Simulation*, vol. 14, no. 5, pp. 1525–1541, 2021.

[11] S. Zhang, B. Du, M. Ge, and Y. Zuo, "Study on the operation of small rooftop wind turbines and its effect on the wind environment in blocks," *Renewable Energy*, vol. 204, no. 21, article 104270, 2021.

[12] X. Ni, "Nursing home wind environment evaluation in northern China - a case study in Dezhou," *IOP Conference Series: Earth and Environmental Science*, vol. 728, no. 1, p. 012013, 2021.

[13] T. Ma and T. Chen, "Classification and pedestrian-level wind environment assessment among Tianjin's residential area based on numerical simulation," *Urban Climate*, vol. 34, no. 11, article 100702, 2020.

[14] C. A. Feng and B. Yw, "Research and application of 3D visualization and Internet of Things technology in urban land use efficiency management," *Displays*, vol. 10, no. 11, pp. 494–506, 2021.

[15] Y. Yang and A. Gou, "Research on wind environment simulation of commercial district based on Phoenics—taking Shanghai Central Building Group as an example," *IOP Conference Series Earth and Environmental Science*, vol. 647, no. 1, article 012193, 2021.

[16] Z. K. Hou, H. L. Cheng, S. W Hou, J. Chen, D. Q. Qi, and Z. B. Liu, "Crack propagation and hydraulic fracturing in different lithologies," *Applied Geophysic*, vol. 16, no. 2, pp. 243–251, 2019.

[17] B. Mo, Z. Ma, H. N. Koutsopoulos, and J. Zhao, "Capacity-constrained network performance model for urban rail systems," *Transportation Research Record*, vol. 2674, no. 5, pp. 59–69, 2020.

[18] V. Leavell, "When do predictions become performative? Evidence from simulation technologies in urban planning," *Academy of Management Annual Meeting Proceedings*, vol. 2020, no. 1, p. 21739, 2020.

[19] C. A. Ku and H. K. Tsai, "Evaluating the influence of urban morphology on urban wind environment based on computational fluid dynamics simulation," *International Journal of Geo-Information*, vol. 9, no. 6, p. 399, 2020.

[20] X. Li, J. Wang, M. Eftekhari et al., "Improvement strategies study for outdoor wind environment in a university in Beijing based on CFD simulation," *Advances in Civil Engineering*, vol. 2020, 14 pages, 2020.